Organic & Biomolecular Chemistry

Cite this: *Org. Biomol. Chem.*, 2012, **10**, 3278

www.rsc.org/obc

PAPER

A NMR and computational study of Smac mimics targeting both the BIR2 and BIR3 domains in XIAP protein

Donatella Potenza,*[a] Laura Belvisi,*[a] Francesca Vasile,[a] Elisabetta Moroni,[a] Federica Cossu[b] and Pierfausto Seneci[a]

Received 24th November 2011, Accepted 2nd February 2012
DOI: 10.1039/c2ob06979b

In this paper we report an extensive NMR analysis of small ligands (Smac mimics) complexed with different constructs of XIAP. The mimics-binding site of XIAP is known as the BIR3 domain – primary, and the linker BIR2 region – secondary site. Interactions between the BIR3 domain and Smac mimics have been extensively studied by X-ray but, as of today, there are scarce data about the interaction between BIR2, or the whole linker–BIR2–BIR3 construct, and Smac mimics. In order to characterize our Smac mimics, we performed a STD NMR study between our 4-substituted, 1-aza-2-oxobicyclo[5.3.0] decane scaffold-based molecules and three different XIAP fragments: single BIR2 and BIR3 domains, and bifunctional linker–BIR2–BIR3. The results were integrated with docking calculations and molecular dynamics simulations. NMR data, which are consistent with biological tests, indicated that the two BIR subunits interact differently with our Smac mimics and suggest that the ligands enter into more intimate contact with the linker–BIR2–BIR3. In conclusion, we observe that the SMAC mimics showed with the construct linker–BIR2–BIR3 a series of NOE contacts that were not observed in the mono-domain ligand: BIR2 or :BIR3 complexes. So, in agreement with the computational models we believe that the linker moieties of the binding site play a key role in the stability of the protein complex.

Introduction

Apoptosis is the cell suicide program that is responsible for the elimination of cells in the organism.[1–3] Deregulation of the apoptotic pathways is linked to a large number of human pathologies such as neurodegenerative disorders, autoimmune diseases and, above all, cancer.[4,5] Thus, an attractive approach for the development of new anticancer therapies is targeting critical apoptosis regulators.

A major mechanism in apoptosis is based upon the sequential activation of a family of cysteine proteases, known as caspases, whose proteolytic activity leads to cell death.[6]

The inhibitor of apoptosis protein (IAP) family is capable of blocking the enzymatic activity of caspases.[7,8] All IAPs contain at least one ~70 residue zinc-binding domain known as the baculovirus IAP repeat (BIR) domain. In particular, the human X-linked inhibitor of apoptosis protein (XIAP, 479 residues), a central apoptosis regulator, contains three BIR domains and a C-terminal RING finger. Structural differences in the BIR domains determine the specific affinities for these proteins, and consequently their role in the regulation of apoptosis. XIAP inhibits apoptosis through direct binding interaction with caspases. In particular, the third BIR domain (BIR3) of XIAP selectively targets caspase-9, whereas the BIR2 domain, together with the linker preceding BIR2, inhibits both caspase-3 and caspase-7.[9–13]

The mechanism by which XIAP inhibits caspases-3, -7, and -9 has been elucidated through X-ray crystallography data of BIR domains cocrystallized with caspases.[10,13] The interaction of XIAP with caspase-9 is stabilized by binding the N-terminus of the small subunit of caspase-9 to a surface groove on the C-terminal helix of BIR3, called IAP Binding Motif (IBM).[13] Structural analyses of the BIR2 domain crystallized in complexes with the caspase-3 and -7, suggest that these proteins are directly inhibited by XIAP through binding of the linker region (18-residue-peptides in length) located on the N-terminal side of BIR2 domain.[10]

In cells, the anti-apoptotic function of XIAP is antagonized by Smac/DIABLO (*s*econd *m*itochondria-derived *a*ctivator of *c*aspases or *d*irect *IA*P *b*inding protein with *l*ow pI).[14,15] Upon receipt of an apoptotic stimulus, Smac is released from the mitochondria; it forms an elongated dimer[14] and targets both the BIR2 and BIR3 domains in XIAP.[16] Biochemical and structural

[a]*Università degli Studi di Milano, Dipartimento di Chimica Organica e Industriale, Centro Interdipartimentale C.I.S.I., Istituto di Scienze e Tecnologie Molecolari-CNR, Via Venezian 21, 20133 Milano, Italy. E-mail: donatella.potenza@unimi.it; Fax: (+)39-02 5031 4072*
[b]*Università degli Studi di Milano, Dipartimento di Scienze Biomolecolari e Biotecnologie, Via Celoria 26, I-20133 Milano, Italy*

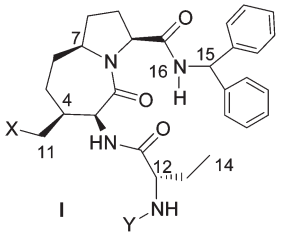

1 X= OH Y= H
2 X= CH_2OH Y= H
3 X= NH_2 Y= H
4 X= CH_2NH_2 Y= H
5 X= $NHCH_2Ph$ Y= H
6 X= CH_2NHCH_2Ph Y= Me
7 X= $NHC(NH_2)NH$ Y= H

Fig. 1 Smac mimetics based on the 1-aza-2-oxo-3-aminobicyclo-[5.3.0]decane-10-carboxylic acid scaffold.

Table 1 Experimentally determined IC_{50} (nM) of compounds **1–7** (fluorescence polarization-based binding assays) on XIAP BIR3 and linker–BIR2–BIR3[24a]

Compound	IC_{50} BIR3	IC_{50} linker–BIR2–BIR3
1	270	290
2	280	70
3	970	110
4	250	86
5	320	72
6	110	27
7	4400	390

studies demonstrated that Smac binds the XIAP BIR3 domain *via* its N-terminal four residues (AVPI) in a way similar to the interaction between caspase-9 and XIAP, suggesting that caspase-9 inhibition by XIAP–BIR3 is achieved by a direct competition with Smac for IBM pocket.[17,18] Smac interferes with the XIAP binding site of caspases-3 and -7 in a different way, although the conclusive understanding of the mechanism by which Smac prevents inhibition by XIAP of caspase-3/-7 remains elusive. However, it is likely that Smac interacts with BIR2 in its IBM pocket as described for the XIAP–BIR3–Smac complex. Actually, BIR2 and BIR3 domains share an amino acid sequence identity of 40% and a very similar fold; in particular, there are some conserved residues in the corresponding IBM pockets. For this reason, unlike caspase-9, an indirect action of Smac in inhibiting the interaction between the linker–BIR2 domain and caspase-3 and -7 has been hypothesized. However, recent studies suggest that additional interactions between XIAP and caspase-3 and -7 involving the IBM groove in the BIR2 domain could contribute to the overall binding affinity and to the inhibitory strength.[11]

Because XIAP blocks apoptosis in a phase where multiple signaling pathways converge, it represents an attractive molecular target for the design of new classes of anticancer drugs. To date, researchers have followed different approaches: one approach focuses on the design of small molecules that target the XIAP BIR2 domain, blocking the interaction of XIAP with caspase-3/7.[19,20] The other approach is to design molecules that target the BIR3 domain, antagonizing the inhibition of caspase-9 by XIAP.[21,22] A third possible approach stems from available data on XIAP–caspases and XIAP–Smac mechanism of interaction: bivalent Smac mimetics targeting both BIR3 and BIR2 domains in the IBM groove may be able to antagonize the interactions between XIAP and all the involved caspases (-9, -7 and -3), thus promoting apoptosis.[23]

In this perspective, a few years ago our group generated a library of 4-substituted aza-bicyclo[5.3.0]decane derivatives of general formula **I** as Smac mimics/XIAP inhibitors (Fig. 1).[24]

These compounds, inspired by the Smac N-terminal AVPI sequence and by the synthetic Smac mimics proposed by Sun *et al.*[22] exhibited different nanomolar/micromolar binding affinities *versus* the BIR3 domain and *versus* the linker–BIR2–BIR3 construct, depending on the 4-substitution.[24a] From the library we selected compounds **1–7** (Fig. 1, Table 1) for an in-depth investigation of their interaction mode with XIAP domains through NMR and computational techniques.

In this paper, the findings of these studies are examined, with the aim to improve the understanding of the structural basis of molecular recognition, and gain an insight into the effects of 4-substitution on binding of our bicyclic Smac mimics to biologically relevant XIAP domains.

NMR experiments were performed by means of STD (saturation transfer difference) techniques[25,26] to investigate the interaction of mimics **1–7** with the BIR2 domain (residues 140–240), the BIR3 domain (residues 241–356) and the linker–BIR2–BIR3 construct of XIAP (residues 124–356), that includes both the BIR2 and BIR3 domains, and the linker (residues 124–139).

Computational models for Smac mimics binding to BIR2, BIR3 and linker–BIR2–BIR3 were built using a combined approach based on docking and molecular dynamics simulations, and the high resolution crystal structures available in the Protein Data Bank[27] for BIR2 and BIR3 domains. Taking into account protein and ligand flexibility, these studies can complement the experimental data obtained by NMR experiments providing a dynamic view of ligand–receptor interactions.

Based on these studies, information about the specific binding mode and the different structural features of 4-substituted bicyclic Smac mimics to target BIR2 and BIR3 domains could be obtained, which may be helpful for designing and synthesizing novel anticancer drugs. In particular, experimental data disclosing the molecular bases of the interaction of Smac mimics of general formula I with the BIR2 domain and the linker–BIR2–BIR3 construct are discussed for the first time in the manuscript in an integrated way with extensive computational simulations.

Results and discussion

Our compounds display different 4-substitutions on the rigid bicyclic scaffold (Fig. 1). These functional groups are selected on the grounds of their ability to experience hydrogen bonding (–OH or $–NH_2$ groups) or π–π interactions ($–CH_2Ph$ group) with the receptor site of the BIR domains. Moreover, we modulated their distance from the scaffold through an alkyl chain.

NMR studies

STD-NMR, together with trNOESY, is one of the most widespread NMR methods for studying the interactions between small ligands and macromolecular receptors.[25] Originally proposed as a technique for the rapid screening of compound libraries, its scope has been extended to include mapping the interaction epitope by determining the ligand regions in contact with the receptor.[26] The method is based on the transfer of saturation from the protein to the bound ligand which in turn, by

Fig. 2 The absolute STD percent for the protons of the diphenylamido group of mimics **1–6** with BIR2 domain: aromatic amide protons (light blue), CH15 (azure), NH16 (blu). Benzylic protons of **5** are shown in yellow.

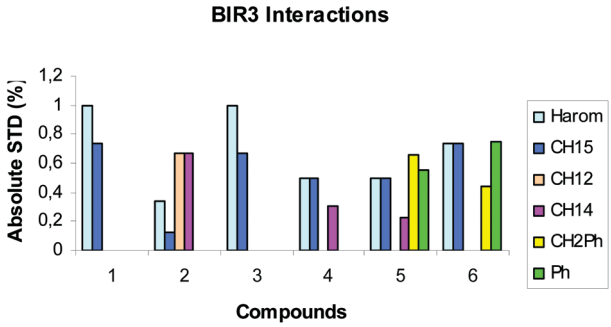

Fig. 3 The absolute STD percent for the protons of Smac mimics **1–6** with BIR3 domain. Interactions between compounds **1–6** and BIR3 seem to feel the effects of the 4-substituents. The protons of the diphenylamido group are indicated in light blue (aromatic protons) and azure (CH15); the protons of the ethylglycine moiety are showed in pink (CH12) and purple (CH14), the protons of the benzylammino group are in yellow (benzylic-CH2) and in green (aromatic protons).

exchange, is moved into solution where it is detected. During the saturation period, progressive saturation transfers from the protein to the ligand protons when the ligand binds to the target. The ligand protons nearest to the protein are most likely to be saturated to the highest degree, and therefore have the strongest signal in the STD spectrum; whereas the ligand protons located further away are saturated to a lower degree, and their STD intensities are weaker. Therefore, the degree of saturation of individual ligand protons (expressed as absolute-STD percent)[25] reflects their proximity to the protein surface and can be used as an epitope-mapping method to describe the target–ligand interactions.

We performed a set of STD-NMR experiments on soluble BIR2–ligand complexes in non-deuterated buffer. The only observed signals were those resulting from the transfer of saturation from bound to free ligand, thus permitting their immediate identification.[28]

Compounds **1–6** showed interactions with the BIR2 domain, while only the guanidine derivative **7** did not interact with BIR2. In particular, in the STD spectrum, all these compounds show a set of signals relative to the diphenylamido group (NH16 at 8.9 ppm; CH15 at 6.0 ppm and aromatic protons in the 7.2–7.4 ppm range). Additionally, compound **5** interacted with the BIR2 domain also through its benzylic protons (both methylenic and aromatic) with the same intensity observed for CH15. This indicates the proximity of these protons to the protein surface in the receptor site. It is important to note that the spectral region corresponding to the aromatic protons is well resolved, and we can discriminate among any phenyl group from 4-substituents or C-terminal amides.

In Fig. 2 the absolute-STD percent of the compounds **1–6** interacting with the BIR2 receptor are reported. Clearly, the most important interactions of compounds **1–6** with the BIR2 domain involve the NH16 protons.

Similar experiments were performed with compounds **1–7** in the presence of the BIR3 domain, or of the linker–BIR2–BIR3 construct. Preliminary NMR studies[24a] were reported for compounds **1**, **3**, **4**, **5** and **7**, while compounds **2** and **6** are analyzed here for the first time.

In addition to C-amide terminus-related interactions, STD spectra performed on samples containing BIR3 and ligands **2**, **4** or **5** show signals relative to 12-ethyl group (0.9 ppm-H14). Compounds **5** and **6** show also a weak interaction of the benzyl moiety (CH_2Ph 4.15 ppm, CH_2Ph 7.4 ppm), once again visible because different aromatic groups can be differentiated. The absolute STD percent for the protons of Smac mimics **1–6** with the BIR3 domain are reported in Fig. 3, while compound **7** did not show any interaction.

Interactions between Smac mimics **1–6** and BIR3 seem to be also influenced by 4-substituents. Moreover, comparison of X-ray complexes between BIR3 and compounds **3** and **4**,[24a] show that the latter, elongated derivative optimizes the interaction between the 4-$CH_2CH_2NH_2$ substitution and Asp309 in the binding site, preserving the EtGly interactions without causing the interaction-poor ligand shift observed for **3** in the BIR3 binding site. Accordingly, elongated compounds **2** and **4** show an additional interaction with EtGly in their NMR spectra, with respect to non-elongated congeners **1** and **3**. In the case of compounds **5** and **6**, both show a strong interaction between BIR3 and the 4-benzyl CH_2 moiety.

The signals observed in the STD spectra for the ligand protons of compounds **1–6** in the presence of linker–BIR2-BIR3 are summarized in Fig. 4. Once again, compound **7** did not show any interaction.

The linker–BIR2–BIR3 construct showed a more complex domain–ligand interaction pattern. As the linker–BIR2–BIR3 construct can accommodate simultaneous interactions with two ligand molecules, by NMR experiments we view their overall result, without discrimination between BIR2- and BIR3-driven interactions. Compounds **1–6** show diphenylamido- and EtGly-related interactions as separately seen for BIR2 and BIR3 domains, likely modulated by 4-substitutions. In addition, the STD spectra in presence of the linker–BIR2–BIR3 construct clearly demonstrate its interaction with some protons of the 4-substituted 1-aza-2-oxobicyclo[5.3.0]decane scaffold itself. Unfortunately, a quantitative and selective analysis of the intensity of individual proton resonances in the 1.5–2.5 ppm region is impeded because of severe signal overlap of the corresponding methylene groups. As these contacts were not observed in the mono-domain ligand:BIR2 or :BIR3 complexes, we reasoned that any additional proton–ligand interaction should indicate an interaction targeted to the linker moieties of the binding site (see also computational studies below).

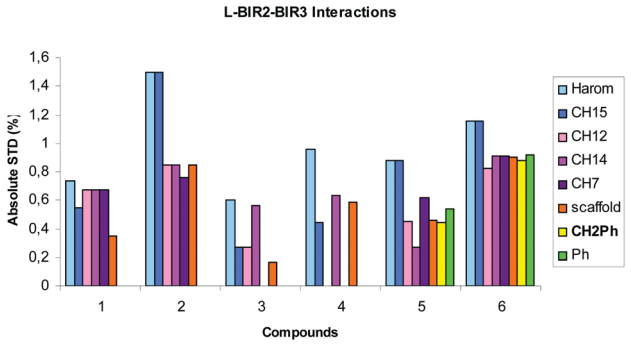

Fig. 4 The absolute STD percent for Smac mimics **1–6** when bound to linker–BIR2–BIR3 construct. The protons of the diphenylamido group are indicated in light blue (aromatic protons) and azure (CH15); the protons of the ethylglycine moiety are showed in pink (CH12) and purple (CH14), some protons of the scaffold are in violet (CH7) and orange (1.5–2.5 ppm region), the protons of the benzylammino group are in yellow (benzylic-CH2) and in green (aromatic protons).

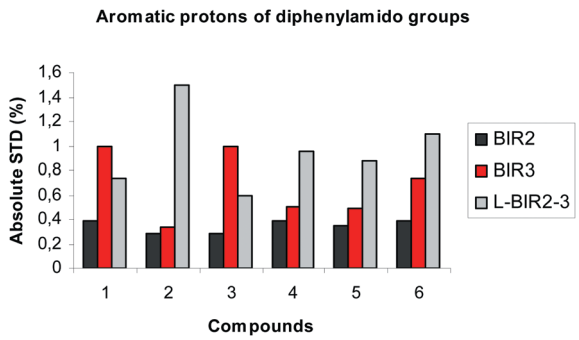

Fig. 5 The absolute STD percent for the aromatic protons of the diphenylamido C-terminus of **1–6** with BIR3 (red), BIR2 (black) and linker–BIR2–BIR3 (grey), respectively.

The recurrent presence of peaks corresponding to the diphenylamido group (NH16 8.8 ppm, Arom 7.2–7.4 ppm, CH15 6.0 ppm) in the STD spectra of Smac mimics **1–6** with any of the three studied XIAP domains indicates that the aforesaid residues interact with all of the caspase-binding domains, as shown in Fig. 5 for the aromatic protons.

As it can be seen, STD effects in presence of BIR3, BIR2 and linker–BIR2–BIR3 are diverse, thus reflecting slightly different binding modes to their sites. For all binders the lowest degree of saturation is obtained with the BIR2 construct. In fact, only the diphenylammido moiety binds to the BIR2 receptor site and the formation of the ligand–protein complex appears to be independent of the 4-substitution. The interactions of our compounds with BIR3 are affected by the presence of polar functional groups in 4-chain. Moreover, at the same functional group, the elongated compounds are closer to the receptor, in fact, we observe an additional interaction with the ethylglicine moiety in compounds **2** and **4** (see Fig. 3). The NMR data for the ligands: linker–BIR2–BIR3 complexes showed more intense and more extensive STD peaks, involving also some protons of the scaffold moiety.

Computational studies

Computational models for Smac mimics binding to BIR2, BIR3 and linker–BIR2–BIR3 were built using a combined approach based on docking and molecular dynamics simulations, and the high resolution crystal structures available for BIR2 and BIR3 domains. As far as the BIR3 domain of XIAP is concerned, X-ray crystallography revealed the structure of this domain in complex with Smac[17b] or several Smac mimics, including the 4-substituted azabicycloalkane compounds **1**, **3** and **4** (Fig. 1).[29] These crystal structures show that the network of protein–ligand interactions displayed by the N-terminal tetrapeptide sequence of Smac/DIABLO in the BIR3 IBM pocket is preserved in the complexes with our mimics. Moreover, the introduction of appropriate 4-substituents on the 1-aza-2-oxobicyclo[5.3.0]decane scaffold allows the formation of some novel interactions with the binding site.[24a,29]

Starting from the high resolution crystal structure of the Smac–BIR3 complex (PDB entry 1G73)[17b] a docking approach has already been set up and applied to a small library of Smac mimics of general formula I. In particular, the 4-substituted compounds of Fig. 1 showed an AVPI like binding mode and additional interactions through their 4-side chains, such as hydrogen bond interactions with the Thr308 and/or the Asp309 BIR3 residues and favourable van der Waals contacts with the protein.[24a]

In this work, starting from the top-ranked binding modes obtained by the docking protocol for ligands **1**, **3** and **4** in the BIR3 domain (shown in Fig. 6 for **1**), explicit solvent molecular dynamics simulations have been performed, to take into account both protein and ligand flexibility and gain insights into ligand–receptor interactions. The majority of intermolecular hydrogen bonds already observed from crystal structures and from docking poses of XIAP–BIR3 complexes with Smac or Smac mimics were conserved throughout the MD simulations, except for two hydrogen bonds (Gln319 side chain with ligand amino terminal group and Trp323 side chain with EtGly carbonyl group) which often show non-optimum structural parameters during the simulation (Table 2).[30]

Moreover, hydrogen bond analysis revealed an interaction pattern for compound **3** which was slightly different from that of ligands **1** and **4**. In fact, the hydrogen bond between the Gly306 carbonyl group and the ligand NH diphenylamido group is formed for the 67% of the simulation by ligand **3** and more than 80% by ligands **1** and **4**. Similarly, the hydrogen bond/salt bridge between the positively charged amino terminal group and the Glu314 carboxylate group is formed in almost 100% of the sampled structures for ligands **1** and **4**, and less than 40% for ligand **3**, whose amino terminal group alternatively interacts with the close negatively charged Asp309 residue. This altered binding mode can be related to the higher IC_{50} value displayed by ligand **3** in fluorescence binding assays with XIAP–BIR3 domain. During the simulations, interactions of the lactam 4-substituents with Thr308 and/or Asp309 side chains are observed, although only the hydrogen bond/salt bridge interactions between the positively charged 4-$CH_2CH_2NH_2$ group in **4** and the Asp309 carboxylate group show optimum geometric parameters in 32% of the sampled structures.

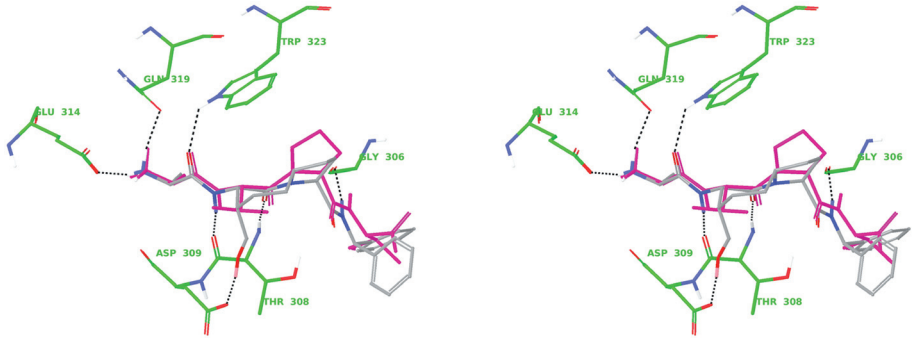

Fig. 6 Stereoview representation of the docking best pose of compound **1** (grey) into the crystallographic (1G73) BIR3 binding site (protein residues involved in hydrogen bond interactions are labelled; C atoms in green, N in blue and O in red) overlaid on the AVPI-bound conformation (magenta). Non-polar hydrogens hidden for better visual representation, intermolecular hydrogen bonds visible (black dashed lines).[31,32]

Table 2 Percentage of hydrogen bonds between Smac mimics **1**, **3**, **4** and BIR3 amino acids, as observed in the MD simulations[30]

		Gly306	Thr308		Glu314	Gln319	Trp323	Asp309	
Mimic		O	NH	O	$O^{\varepsilon1}$–$O^{\varepsilon2}$	$O^{\varepsilon1}$	$N^{\varepsilon1}H$	O	$O^{\delta1}$–$O^{\delta2}$
Ter $NH3^+$	**1**				100	0		55	0
	3				38	1		37	27
	4				100	1		37	1
EtGly C═O	**1**						21		
	3						15		
	4						22		
Lactam NH	**1**			100					
	3			100					
	4			100					
Lactam C═O	**1**		100						
	3		100						
	4		100						
NH16	**1**	83							
	3	67							
	4	86							
4-Subst.	**1**								1
	3								2
	4								32

So far, despite several efforts, X-ray crystallography has failed to reveal the structure of the XIAP–BIR2 domain in complex with Smac or Smac mimics. For this reason, to obtain some insights into BIR2/Smac mimics interactions, we decided to build a computational model for Smac mimic binding to BIR2 IBM pocket using a combined approach based on docking and molecular dynamics simulations.

Starting from the high resolution crystal structure of XIAP–BIR2 in complex with caspase 3 (PDB entry 1I30, subunit E),[10b] an initial guess of the complex structure was generated by flexible docking of the Smac mimic **3** in the rigid BIR2 IBM pocket. Then, mutual ligand–receptor structural adjustment as well as reorganization of the ligand–protein interaction network (in a complexed state) have been achieved by running 5 ns explicit solvent molecular dynamics simulation of the complex and allowing both protein and ligand flexibility. The structures sampled during the production time were clustered according to similarity in backbone torsion angles of the BIR2 binding site, and the central structure of the most populated cluster was used as rigid receptor in flexible ligand docking calculations of Smac mimics of general formula I. Binding modes similar to those of the mimics to the BIR3 domain were observed, are likely to be related to the high degree of sequence and structural homology of the IBM groove in the BIR2 and BIR3 domains.[29a] In particular, intermolecular hydrogen bond patterns in the BIR2–Smac mimetic complexes are closely similar to those observed in the BIR3 domain complexes, involving the same ligand functional groups and the BIR2 residues corresponding to a structure-based alignment of the IBM groove BIR2 and BIR3 amino acids (Lys206, Lys208, Asn209, Asp214, Glu219, His223).

Starting from the top-ranking binding modes obtained by the docking calculations for ligands **1**, **3** and **4** in the BIR2 domain (shown in Fig. 7 for **1**), extensive explicit solvent molecular dynamics simulations of the complexes have been

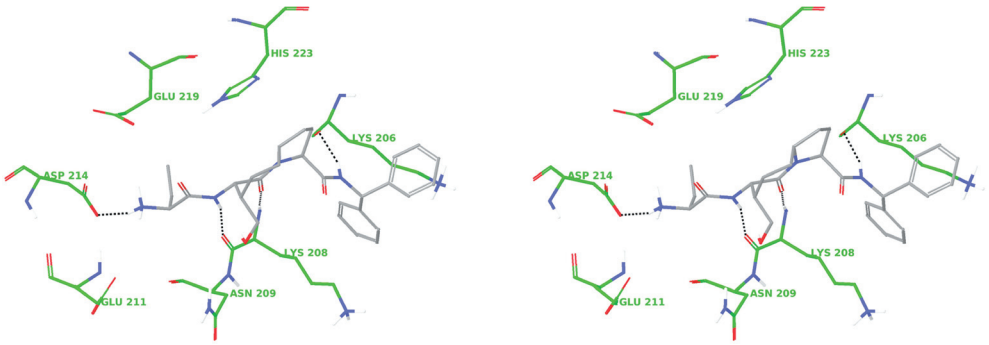

Fig. 7 Stereoview representation of the docking best pose of compound **1** (grey) into the BIR2 binding site (protein residues involved in hydrogen bond interactions are labelled; C atoms in green, N in blue and O in red). Non-polar hydrogens hidden for better visual representation, intermolecular hydrogen bonds visible (black dashed lines).[31,32]

Table 3 Percentage of hydrogen bonds between Smac mimics **1**, **3**, **4** and BIR2 amino acids, as observed in the MD simulations[30]

		Lys206	Lys208		Asp214	Glu219	His223	Asn209	
Mimic		O	NH	O	$O^{\delta1}$–$O^{\delta2}$	$O^{\varepsilon1}$–$O^{\varepsilon2}$	$N^{\varepsilon1}H$	O	$O^{\delta1}$
Ter $NH3^{+a}$	**1**				84	2		37	0
	3				100	22		26	0
	4				100	43		23	0
EtGly C═O	**1**						14		
	3						14[b]		
	4						39		
Lactam NH	**1**			100					
	3			99					
	4			100					
Lactam C═O	**1**		100						
	3		99						
	4		100						
NH16	**1**	78							
	3	81							
	4	95							
4-Subst.	**1**								0
	3								3
	4								50

[a] The amino terminal group of **1**, **3** and **4** forms H-bonds also with Glu211 side chain (35%, 43% and 28% of the sampled structures, respectively). [b] The EtGly carbonyl group of mimic **3** also forms a H-bond with Arg222 side chain (13% of the sampled structures).

performed for a dynamic insight into ligand–receptor interactions.

Analysis of MD trajectories revealed that the ligand terminal amine maintains the hydrogen-bonded salt bridge to the Asp214 side chain (Glu314 in BIR3) and may form other stabilizing electrostatic/H-bond interactions with Glu 211 (Lys311 in BIR3) and Glu219 (Gln 319 in BIR3) side chains, and with Asn209 backbone carbonyl group (Table 3). BIR2 Lys208 may establish the same hydrogen-bonded network with Smac mimics displayed by BIR3-Thr308, as well as the hydrogen bond of the ligand diphenylamido NH with the Lys206 carbonyl group (Gly306 in BIR3) appears to be conserved in BIR2 complexes.

Finally, hydrogen bond analysis suggested that His223 and Arg 222 side chains may hydrogen-bond to the ligand EtGly carbonyl group, and that BIR2 residue Asn209 may hydrogen-bond to the lactam 4-substituents, although only the hydrogen bond interactions between the 4-$CH_2CH_2NH_2$ group in **4** and the Asn209 side chain show optimum geometric parameters in 50% of the sampled structures.

The electrostatic/H-bond interactions displayed by Smac mimics in the BIR2 domain, particularly by ligands **3** and **4**, may be one of the factors contributing to their enhanced affinity for the L–BIR2–BIR3 construct. Moreover, according to NMR-STD experiments (Fig. 2 and 3), interactions of Smac mimics with BIR3 computed from MD trajectories are modulated by 4-substituents more than in BIR2.

The distances between the H15 proton of the ligand diphenylamido group and each hydrogen atom of the BIR2 or BIR3

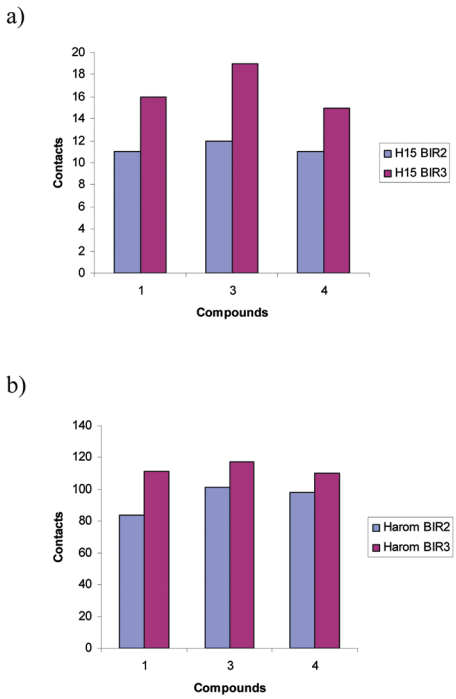

Fig. 8 Mean number of contacts of (a) H15 and (b) the aromatic diphenylamido protons with the BIR2 or BIR3 binding site protons calculated from the MD simulations of **1**, **3** and **4**.

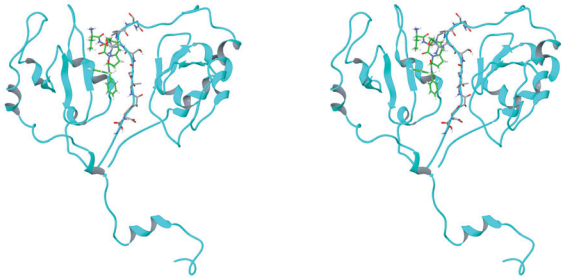

Fig. 9 A snapshot from the MD simulation of **1** (green tube representation) in the BIR2 domain of the L–BIR2–BIR3 construct (cyan ribbon representation). Residues Ser241–Asn249 are shown as grey tube representation overlaid on the backbone trace.

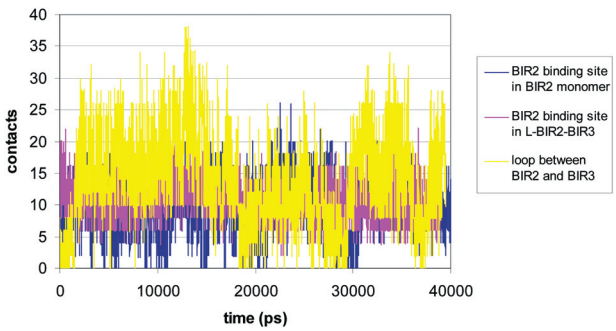

Fig. 10 Number of contacts of the scaffold protons of **1** calculated from the MD simulations of **1** with the BIR2 domain or the L–BIR2–BIR3 construct (blue trace: contacts of the scaffold with the BIR2 binding site in the BIR2 domain; magenta trace: contacts of the scaffold with the BIR2 binding site in the L–BIR2–BIR3 construct; yellow trace: contacts of the scaffold with residues Ser241–Asn249 of the BIR2–BIR3 connecting loop). The simulation time in ps is reported on the *x*-axis and the time interval between frames is 10 ps.

binding site amino acids were analysed throughout the production time of MD simulations. According to STD results (Fig. 2 and 3), calculation of distance values less than 4 Å showed more favourable Van der Waals contacts in BIR3 than in BIR2 domain (Fig. 8a). Identical results were obtained from the analysis of the distances between the aromatic protons of the diphenylamido group and the binding site protons (Fig. 8b), in agreement with experimental NMR data (Fig. 5). These differences may be related to the distinct characteristics of the binding sites and/or of the ligand binding modes.

Finally, a computational binding model of the linker–BIR2–BIR3 construct (residues 127–345) in complex with the Smac mimic **1** was built using the crystal structure of a cyclic, bivalent Smac mimic in complex with the XIAP BIR3 domain (PDB entry 2VSL)[33] and the crystal structure of the XIAP BIR2 domain in complex with caspase 3 (PDB entry 1I3O).[10b] Following the procedure described in the experimental section, a starting structure of the complex was obtained and then refined and investigated through extensive molecular dynamics (MD) simulations using the Amber program.

In the modeled structures, the binding pockets of the two BIR domains stay together to form one large pocket that surrounds the ligand, and show distance values between the center of mass of BIR2 and BIR3 in the 26–28 Å range. The analysis of MD trajectories revealed that the interaction between BIR2 or BIR3 in the protein and the Smac mimic **1** is very similar to that observed previously in the structures of the complexes with one domain. Importantly, the sampled structures shed light on the contacts experienced by ligand scaffold protons in the linker–BIR2–BIR3 construct (see STD-NMR experiments, Fig. 4), showing more favourable contacts with some protons in the connecting loop (residues S241–N249, in particular with protons of Val244 and Arg248) between BIR2 and BIR3 domains than with binding site protons (Fig. 9 and 10).

The number of contacts of the ligand scaffold protons (shown on the *y*-axis in Fig. 10) was calculated in each snapshot of the MD trajectory by counting the distance values less than 4 Å between these protons and BIR2 binding site protons, both in the simulations with the BIR2 domain alone (trace blue) and with the L–BIR2–BIR3 construct (magenta trace). The similar trend observed from the analysis of the blue and magenta traces suggests comparable Van der Waals contacts of ligand scaffold protons with the binding site during MD simulations in both the constructs. Higher numbers of favourable Van der Waals contacts are calculated during the simulation with the L–BIR2–BIR3 construct between ligand scaffold protons and some protons in the connecting loop between BIR2 and BIR3 domains (yellow trace), suggesting a role of the S241–N249 linker region in the interaction with Smac mimics and offering an explanation of the NOE contacts experienced by scaffold protons in the bifunctional XIAP construct.

Conclusions

In this paper we report an extensive NMR analysis of small ligands (Smac mimics) complexed with different constructs of XIAP. The mimics-binding site of XIAP is known to be the BIR3 domain – primary, and the linker-BIR2 region – secondary site. Interactions between the BIR3 domain and Smac mimics has been extensively studied by X-ray but, as of today, there are scarce data about the interaction between BIR2, or the whole linker–BIR2–BIR3 construct, and Smac mimics.

In order to characterize our Smac mimics, we performed a STD NMR study between our 4-substituted, 1-aza-2-oxobicyclo [5.3.0]decane scaffold-based molecules and three different XIAP fragments: single BIR2 and BIR3 domains, and bifunctional linker–BIR2–BIR3. The results were integrated with docking calculations and molecular dynamics simulations.

NMR data indicated that the two BIR subunits interact differently with our Smac mimics. In particular, the diphenylamido group (NH16, H15 and Aromatic) of these compounds is the only interaction observed with BIR2. As for BIR3, the 4-substitution is important to modulate the binding; the potency of the compounds increases when the epitope of the molecule involves also ethylglycine moiety or the 4 benzylic substituent. Moreover, at the same functional group, the elongated compounds are closer to the receptor (*e.g.*, 2 *vs*. 1 and 3 *vs*. 4). The STD-NMR experiments performed with the construct linker–BIR2–BIR3 show a different picture. First of all, interactions are more intense and more extensive involving also some protons of the scaffold moiety. NMR and computational studies show that the interaction with Smac mimics is also mediated by strong hydrophobic contacts between 1-aza-2-oxobicyclo[5.3.0]decane scaffold protons and the linker in the construct linker–BIR2–BIR3.

The NMR data suggest that the ligands enter into more intimate contact with the linker–BIR2–BIR3.

In conclusion, we observe that the SMAC mimics **1**–**6** showed with the construct linker–BIR2–BIR3, a series of STD contacts that were not observed in the mono-domain ligand:BIR2 or :BIR3 complexes. So, in agreement with the computational model we believe that the linker moieties of the binding site plays a key role in the stability of the protein complex.

Materials and methods

Protein constructs used in this work were cloned, expressed and purified according to the protocol described in ref. 29.

NMR methods

All protein/ligand samples were prepared in a 1 : 90 protein–ligand ratio. Typically, the final concentration of the samples was 5 mM in Smac mimic and 0.055 mM in proteins, and the final volume was 200 μL. The buffer used for BIR3 and full length XIAP samples was 100 mM NaCl, 10 mM deuterated Tris, 5 mM deuterated DTT in D_2O or H_2O with 10% D_2O, pH 7.3. The buffer used for BIR2 and linker–BIR2–BIR3 was 20 mM, 200 mM, 10 mM deuterated DTT in H_2O with 10% D_2O, pH 6.5. The BIR domains are characterized by a zinc-finger motif which is essential for the correct folding of BIR domains. The zinc ion was taken up from the *E. coli* cytoplasm after IPTG induction. Crystallization conditions and NMR buffer were the same and did not contain zinc ions and crystallization trials were performed with a correctly folded protein construct. ^{1}H NMR STD experiments were performed at 600 MHz on a Bruker Avance spectrometer. The probe temperature was maintained at 298 K. In the STD experiment water suppression was achieved by WATERGATE 3-9-19 pulse sequence. The on-resonance irradiation of the protein was performed at a chemical shift of −0.05 ppm. Off-resonance irradiation was applied at 200 ppm, where no protein signals were visible. Selective presaturation of the protein was achieved by a train of Gauss shaped pulses of 49 ms length each. The total length of the saturation train was 2.94 s.

Intensities of all STD effects (absolute STD) were calculated by division through integrals over the respective signals in STD NMR reference spectra. The different signal intensities of the individual protons are best analyzed from the integral values in the reference and STD spectra, respectively. $(I_0 - I_{sat})/I_0$ is the fractional STD effect, expressing the signal intensity in the STD spectrum as a fraction of the intensity of an unsaturated reference spectrum. In this equation, I_0 is the intensity of one signal in the off-resonance or reference NMR spectrum, I_{sat} is the intensity of a signal in the on-resonance NMR spectrum, and $I_0 - I_{sat}$ represents the intensity of the STD NMR spectrum.

Computational methods

Docking methodology. Automated docking calculations were performed using Glide v4.5 (Grid-based Ligand Docking with Energetics) within the framework of the Schrödinger suite of programs.[34] Starting from the high resolution crystal structure of the Smac–BIR3 complex (PDB code 1G73)[17b] a docking protocol has been set up using the chain D of the BIR3 protein, the four initial residues Ala 1-Val 2-Pro 3-Ile 4 (Ile4 capped as *N*-methyl amide) of the co-crystallized Smac chain A, and the Protein Preparation Wizard of the graphical user interface Maestro. The grid generation step started from the resulting structure of the complex. The center of the grid-enclosing box was defined by the center of the bound ligand. The enclosing box dimensions, which are automatically deduced from the ligand size, fit the entire active site. For the docking step, the size of the bounding box for placing the ligand center was set to 12 Å. No further modifications were applied to the default settings working in a standard precision mode (SP). The GlideScore function was used to select 10 poses for each ligand. Glide was initially tested for its ability to reproduce the crystallized binding geometry of the AVPI peptide. The program was successful in reproducing the experimentally found binding mode of this compound, as it corresponds to the best-scored pose.

Construction of Smac mimics/XIAP–BIR3 complex. The docking procedure was used to obtain models of Smacs mimics **1**, **3** and **4** bound to BIR3 IBM pocket (residues 256–345); highest docking-score complexes have been compared with the corresponding crystal structures in order to check their accuracy; finally these structures were used as the starting point for Molecular Dynamics simulations.

Construction of Smac mimics/XIAP–BIR2 complex. Models of Smac mimics **1**, **3** and **4** bound to BIR2 IBM pocket have been obtained using a combined approach based on docking and molecular dynamics simulations.

Starting from the high resolution crystal structure of XIAP–BIR2 in complex with caspase 3 (PDB entry 1I30, subunit E),[10b] Smac mimic **3** was placed in the BIR2 IBM pocket (residues 127–237) using a docking procedure similar to the methodology previously described.

The resulting complex was refined by running 5 ns explicit solvent molecular dynamics simulation, according to the procedure described below.

Structures sampled every 10 ps during the production time were clustered using the program *g_cluster* from the GROMACS package, after the trajectories were translated to the suitable format (methods *gromos*, cutoff *0.25*). The central structure of the most populated cluster was used as rigid receptor in flexible ligand docking of Smac mimics **1**, **3**, and **4** using Glide. Highest docking-score complexes were used as starting structures for molecular dynamics simulations.

Construction of the Smac mimics/linker–BIR2–BIR3 complex. The model of the linker–BIR2–BIR3 construct (residues 127–345) was built as previously described;[33] Smac mimic **1** was placed in this structure in three different positions, namely in BIR2, in BIR3 and in both domains using the docking procedure described above. Highest docking-score complexes were further refined through extensive molecular dynamics simulations.

Molecular dynamics simulations. All MD simulations were performed using the AMBER 9.0 package[35] with the ff03 force field, under periodic boundary conditions. In order to remove any bad contacts, every complex was initially minimized *in vacuo* by multiple minimizations (200 steps steepest descent plus 200 steps conjugate gradient). After this, each system was solvated in a cubic box large enough to contain 1 nm of solvent molecules around the complex. The TIP3P water model was used for solvation.[36] Charges on side chains were chosen to correspond to a pH value of 7. Na^+ counterions were added to ensure electroneutrality. In order to allow the solvent molecules to relax around the solute the system was minimized keeping the complex fixed and just minimizing the positions of water and ions (500 steps steepest descent plus 200 steps conjugate gradient); a cut-off of 1 nm was used to compute the non-bonded interactions. Particle Mesh Ewald summation method (PME) was used to deal with long-range Coulomb interactions.[37] The Berendsen's algorithm was used to control temperature and pressure.[38] After this minimization stage holding the solute fixed, the entire system was energy minimized (1500 steps steepest descent plus 1000 steps conjugate gradient). Afterwards, the temperature of the system was slowly brought to the desired value of 300 K using a weak restrain on the solute at constant volume in order to avoid any fluctuations. Finally, a last 100 ps equilibration NPT process was performed with no restrictions on the system. This protocol resulted in 40 ns MD runs for each complex. Docking calculations required a few minutes for each ligand on a monoprocessor workstation (Intel Xeon 2.40 GHz). As far as the MD simulation time is concerned, 40 ns of the monomeric solvated systems (about 21 000 atoms) required 42 days on the HP Cluster Lagrange at Cilea (Consorzio Interuniversitario Lombardo per l'Elaborazione Automatica) using 8 Intel Xeon QuadCore 3.166 GHz processors and 54 days for the solvated dimeric systems (about 43 000 atoms).

In the XIAP protein a zinc ion is coordinated to three cysteines and one histidine. The zinc ion was treated using the cationic dummy approach.[39] This method consists of modeling the zinc ion as a tetrahedral divalent cation with a zinc nucleus and four dummy atoms placed at the four apices of the tetrahedron, in order to impose the right orientation required for the coordinated residues. The zinc atom is bound covalently to the dummy atoms and interacts with the protein only through van der Waals forces, while the dummies interact with the protein only through electrostatic forces. Parameters used to describe the metal and dummies, and their charge and bonding properties are detailed in ref. 39.

Acknowledgements

The authors thank Prof. Anna Bernardi and Prof. Carlo Scolastico for helpful discussions, E. Mastrangelo and M. Milani for protein expression and CILEA for computing facilities. The authors also gratefully acknowledge MUR, CNR and Comune di Milano (Convenzione 55/2008) for financial support.

References

1 D. R. Green, *Cell*, 2000, **102**, 1–4.
2 S. W. Fesik, *Cell*, 2001, **103**, 273–282.
3 Y. Shi, *Nat. Struct. Biol.*, 2001, **8**, 394–401.
4 N. A. Thornberry and Y. Lazebnik, *Science*, 1998, **281**, 1312–1316.
5 B. B. Wolf and D. R. Green, *J. Biol. Chem.*, 1999, **274**, 20049–20052; S. W. Lowe and A. W. Lin, *Carcinogenesis*, 2000, **21**, 485–495.
6 G. S. Salversen and J. M. Abrams, *Oncogene*, 2004, **23**, 2774–2784.
7 Q. L. Deveraux and J. C. Reed, *Genes Dev.*, 1999, **13**, 239–252.
8 E. C. La Casse, S. Baid, R. G. Korneluk and A. E. Mackenzie, *Oncogene*, 1998, **17**, 3247–3259.
9 J. Chai, E. Shiozaki, S. M. Srinivasula, Q. Wu, P. Dataa, E. S. Alnemri and Y. Shi, *Cell*, 2001, **104**, 769–780.
10 (*a*) Y. Huang, Y. C. Park, R. L. Rich, D. Segal, D. G. Myszka and H. Wu, *Cell*, 2001, **104**, 781–790; (*b*) S. J. Riedl, M. Renatus, R. Schwarzenbacher, Q. Zhou, C. Sun, S. W. Fesik, R. C. Liddington and G. S. Salveson, *Cell*, 2001, **104**, 791–800.
11 F. L. Scott, J. B. Denault, S. J. Riedl, H. Shin, M. Renatus and G. S. Salvesen, *EMBO J.*, 2005, **24**, 645–655.
12 S. M. Srinivasula, R. Hegde, A. Saleh, P. Dataa, E. Shiozaki, J. Chai, R. A. Lee, P. D. Robbins, T. Fernandes-Alnemri, Y. Shi and E. S. Alnemri, *Nature*, 2001, **410**, 112–116.
13 E. N. Shiozaki, J. Chai, D. J. Rigotti, S. J. Riedl, P. Li, S. M. Srinivasula, E. S. Alnemri, R. Fairman and Y. Shi, *Mol. Cell*, 2003, **11**, 519–527.
14 J. Chai, C. Du, J. W. Wu, S. Kyin, X. Wang and Y. Shi, *Nature*, 2000, **406**, 855–862.
15 C. Y. Du, M. Fang, Y. C. Li, L. Li and X. D. Wang, *Cell*, 2000, **102**, 33–42; A. M. Verhagen, P. G. Ekert, M. Pakusch, J. Silk, L. M. Connolly, G. E. Reid, L. R. Moritz, R. J. Simpson and D. L. Vaux, *Cell*, 2000, **102**, 43–52.
16 E. N. Shiozaki and Y. Shi, *Trends Biochem. Sci.*, 2004, **29**, 486–494.
17 (*a*) Z. Liu, C. Sun, E. T. Olejniczak, R. P. Meadows, S. F. Betz, T. Oost, J. Herrman, J. C. Wu and S. W. Fesik, *Nature*, 2000, **408**, 1004–1008; (*b*) G. Wu, J. Chai, T. L. Suber, J. W. Wu, C. Du, X. Wang and Y. Shi, *Nature*, 2000, **408**, 1008–1012.
18 R.A. Kipp, M. A. Case, A. D. Wist, C. M. Cresson, M. Carrellll, E. Griner, A. Wiita, P. A. Albiniak, J. Chai, Y. Shi, M. F. Semmelhack and G. L. McLendon, *Biochemistry*, 2002, **41**, 7344–7349.
19 T. Y. Wu, K. W. Wagner, B. Bursulaya, P. G. Schultz and Q. L. Deveraux, *Chem. Biol.*, 2003, **10**, 759–767.

20 A. D. Schimmer, *et al.*, *Cancer Cell*, 2004, **5**, 25–35.
21 H. Sun, Z. Nikolovska-Coleska, J. Lu, S. Qiu, C.-Y. Yang, W. Gao, J. Meagher, J. Stuckey and S. Wang, *J. Med. Chem.*, 2006, **49**, 7916–7920.
22 H. Sun, Z. Nikolovska-Coleska, C.-Y. Yang, L. Xu, M. Liu, Y. Tomita, H. Pan, Y. Yoshioka, K. Krajewski, P. P. Roller and S. Wang, *J. Am. Chem. Soc.*, 2004, **126**, 16686–16687.
23 H. Sun, Z. Nikolovska-Coleska, J. Lu, J. L. Meagher, C.-Y. Yang, S. Qiu, Y. Tomita, Y. Ueda, S. Jiang, K. Krajewski, P. P. Roller, J. A. Stuckey and S. Wang, *J. Am. Chem. Soc.*, 2007, **129**, 15279–15294.
24 (*a*) P. Seneci, A. Bianchi, C. Battaglia, L. Belvisi, M. Bolognesi, A. Caprini, F. Cossu, E. de Franco, M. de Matteo, D. Delia, C. Drago, A. Khaled, D. Lecis, L. Manzoni, M. Marizzoni, E. Mastrangelo, M. Milani, I. Motto, E. Moroni, D. Potenza, V. Rizzo, F. Servida, E. Turlizzi, M. Varrone, F. Vasile and C. Scolastico, *Bioorg. Med. Chem.*, 2009, **17**, 5834–5856; (*b*) C. Scolastico, L. Manzoni, P. Seneci, L. Belvisi, D. Delia, M. Bolognesi, E. Mastrangelo, M. Milani, I. Motto and C. Drago, *EPO* 7021843, 2007.
25 M. Mayer and B. Meyer, *Angew. Chem.*, 1999, **111**, 1902–1906; M. Mayer and B. Meyer, *Angew. Chem., Int. Ed.*, 1999, **38**, 1784–1788; B. Meyer and T. Peters, *Angew. Chem.*, 2003, **115**, 864–890; B. Meyer and T. Peters, *Angew. Chem., Int. Ed.*, 2003, **42**, 864–890.
26 M. Mayer and B. Meyer, *J. Am. Chem. Soc.*, 2001, **123**, 6108–6117.
27 www.pdb.org
28 Without any protein present, STD spectra did not contain ligand signals, because saturation transfer does not occur without the protein.
29 (*a*) E. Mastrangelo, F. Cossu, M. Milani, G. Sorrentino, D. Lecis, D. Delia, L. Manzoni, C. Drago, P. Seneci, C. Scolastico, V. Rizzo and M. Bolognesi, *J. Mol. Biol.*, 2008, **384**, 673–689; (*b*) F. Cossu, E. Mastrangelo, M. Milani, G. Sorrentino, D. Lecis, D. Delia, L. Manzoni, P. Seneci, C. Scolastico and M. Bolognesi, *Biochem. Biophys. Res. Commun.*, 2009, **378**, 162–167.
30 The percentage of H-bond is the percent fraction of conformations sampled during the simulation in which donor hydrogen–acceptor heteroatom distance <2.5 Å. Hydrogen bond analysis has been performed by means of Amber "hbond" analysis tool, using a distance cutoff of 2.5 Å for the DH···A distance. Mean D–H···A angle values >140° (often >160°) have been obtained for the monitored H-bonds.
31 The picture has been generated by means of the Maestro graphical interface and intermolecular hydrogen bonds have been drawn according to the following criteria: maximum DH A distance 2.5 Å, minimum D–H···A donor angle 120°, minimum H···A–R acceptor angle 90°.
32 Maestro, version 8.0, Schrödinger, LLC, New York, NY, 2007.
33 Z. Nikolovska-Coleska, J. L. Meagher, S. Jiang, C.-Y. Yang, S. Qiu, P. P. Roller, J. A. Stuckey and S. Wang, *Biochemistry*, 2008, **47**, 9811–9824.
34 Glide, version 4.5, Schrödinger, LLC, New York, NY, 2007.
35 D. A. Case, T. A. Darden, T. E. I. Cheatham, C. L. Simmerling, J. Wang, R. E. Duke, R. Luo, K. M. Merz, D. A. Pearlman, M. Crowley, *et al.*, AMBER 9, University of California, 2006.
36 W. L. Jorgensen, J. Chandrasekhar, J. Madura, R. W. Impey and M. L. Klein, *J. Chem. Phys.*, 1983, **79**, 926–935.
37 T. Darden, D. York and L. Pedersen, *J. Chem. Phys.*, 1993, **98**, 10089–10092.
38 H. J. C. Berendsen, J. P. M. Postma, W. F. v. Gunsteren, A. D. Nola and J. R. Haak, *J. Chem. Phys.*, 1984, **81**, 3684–3690.
39 Y. Pang, K. Xu, J. El Yazla and F. Prendergast, *Protein Sci.*, 2000, **9**, 1857–1865.